Evaluation of open-access global digital elevation models (AW3D30, SRTM and ASTER) for flood modelling purposes

Laurent Guillaume Courty [a, b], Julio César Soriano-Monzalvo [a, c], and Adrián Pedrozo-Acuña [a,*]

[a]Instituto de Ingeniería, Universidad Nacional Autónoma de México, Circuito Escolar, Ciudad Universitaria, 04510 Ciudad de México, Mexico
[b]Department of Geography, Loughborough University, Loughborough LE11 3TU, United Kingdom
[c]Comisión Nacional del Agua, Avenida Insurgentes Sur 2416, Copilco El Bajo, 04340 Ciudad de México, Mexico
[*]Correspondance to: apedrozoa@ii.unam.mx

June 2018

Keywords: Digital Elevation Model, flood, ALOS.

Abstract

Elevation data in the form of Digital Elevation Model (DEM) is a key piece of information for the accurate representation of topographic controls exerted in hydrologic and hydraulic models. Many practitioners rely on open-access global datasets usually obtained from space-borne survey due to the cost and sparse coverage of sources of higher resolution. In may 2016 the Japan Aerospace eXploration Agency (JAXA) publicly released an open-access global Digital Surface Model (DSM) at an horizontal resolution of 30 m, the ALOS World 3D-30m (AW3D30). So far no published study did an in-depth assessment of the flood modelling capabilities of this new product. The purpose of this investigation is to 1) present an assessment of the capacity of the AW3D30 for flood modelling purposes and 2) to compare its performance with regards to computed water levels and flood extent maps calculated using other freely available 30 m DEM for model setup (e.g. SRTM and ASTER). For this comparison, the reference to reality is given by the water levels and flood extent maps computed with the same numerical model but using a Light Detection And Ranging (LiDAR) based Digital Terrain Model (DTM) (5 m of spatial resolution re-sampled to 30 m). The numerical model employed in this investigation is based on a damped partial inertia approximation of the Saint-Venant equations on a regular raster grid, which is forced with a simple and synthetic rainfall storm event. Numerical results using different elevation data in model setup are compared for two regions with contrasting topographic gradients. Results with regards to water depth and flood extent show that AW3D30 performs better than the SRTM DEM. Notably, in the case of mountainous regions, the results derived with the AW3D30 are comparable in skill to those obtained with a LiDAR derived DSM, suggesting its suitability in the numerical reproduction of flood events. This encouraging performance paves the way to more accurate modelling for both data-scarce regions and global flood models.

1 Introduction

In the last decade, inundations where the disaster that affected more people in the world (IFRC, 2016). In the future and under conditions driven by climate change, the population exposed to floods is likely to increase (Hirabayashi et al., 2013). Hallegatte et al. (2013) predict that without improvement in flood defences, the flood-related damages in coastal cities alone could reach USD $1 trillion a year by 2050.

A common way to assess the level of exposure to these hydrometeorological events is to employ hydrological and hydraulic models that describe the physics of the overland flows. However, as the level of complexity of these numerical tools increases, the data requirements for the model setup also increase. The recent diffusion of remotely sensed data for both hydrological variables (e.g. precipitation (Hou et al., 2014)) and topographic information (Sanders, 2007) has enabled an increase in the level of sophistication of numerical tools and approaches used by hydrologists, favouring the use of bidimensional models (Bates, 2004).

Among the most important datasets that are needed to carry out a proper flood inundation modelling exercise, are hydrometeorological observations (i.e. rating curves, rainfall, runoff) to define boundary and initial conditions, topographic data for the description of the catchment geometry, and flood extent maps or high flood marks for model calibration and validation (Di Baldassarre, 2012). Evidently, the level of accuracy and resolution in all these datasets have an effect on the reliability of the model results. For instance, in the case of topographic data, a commonly used input is the DEM, which represents a gridded product with values of elevation. This was actually proved in a numerical exercise presented by Horritt and Bates (2001), whom showed that inundation models of large rivers have a maximum performance at a spatial resolution of 50 m. Their numerical results were compared in terms of identified affected areas against those detected by satellite imagery. Indeed, there is a wide recognition that accurate DEM are critical for accurate flood modelling and management (Jarihani et al., 2015; Bates, 2004; Cook and Merwade, 2009).

DEM are often derived using remote sensing techniques, such as LiDAR surveys. These airborne laser altimetry datasets enable a numerical description of the floodplains with planimetric and altimetric resolution of less 1 m and less than 0.2 m (Hodgson and Bresnahan, 2004), respectively. Therefore, along with the use of Geographical Information System (GIS), its use has encouraged the utilisation of bidimensional hydraulic models in flood modelling studies (Marks and Bates, 2000; Sanders, 2007). In the last 20 years, the development of aerial LiDAR has been a game-changer in the field of flood modelling thanks to its ability to quickly survey large areas at relatively high vertical accuracy (Hodgson and Bresnahan, 2004) and spatial resolution. However, in some countries, its utilisation has not been widespread due to its high cost. On the other hand, there has also been a clear improvement in the availability of space-borne topographic data that have near-global and are free to use. Indeed, recent studies report the use of this type of datasets to support flood modelling activities (Jarihani et al., 2015; Yan et al., 2015a; Yan et al., 2015b).

This is the case of the Shuttle Radar Topography Mission (SRTM), which produced a near-global dataset with a spatial resolution of 1″ (around 30 m) (Farr et al., 2007). This dataset was acquired using Interferometric Synthetic-Aperture Radar (InSAR) during an 11 days mission aboard the National Aeronautics and Space Administration (NASA) space shuttle in February 2000. The first version of that DSM was released in 2003 and cover an area of Earth between 60° north and 56° south. Most of the world was released at a resolution of 3″, while the United States of America (USA) was covered at a spatial resolution of 1″. The availability this product made it one of the most commonly used global DEM for hydraulic and hydrologic modelling of large rivers (e.g. Schumann et al., 2010; Pedrozo-Acuña et al., 2012; Pedrozo-Acuña et al., 2015; Sampson et al., 2015; Yan et al., 2015b). For instance, LeFavour and Alsdorf (2005) demonstrated its application to derive useful hydraulic parameters in the Amazon river, such as water surface slope and discharge. Although it is still recognised that the dataset has a low vertical accuracy (around 6 m), the data have proven to be of great use for flood modelling studies, especially in cases where more detailed topographic data (e.g. LiDAR) are not available (e.g. Pedrozo-Acuña et al., 2012; Pedrozo-Acuña et al., 2015). During the year 2015, the US government released the 1″ version of the SRTM, which is no longer limited to US territories.

Additionally, another well-known global and free dataset for elevation is that produced by a cooperation of the Ministry of Economy, Trade, and Industry (METI) of Japan and the NASA. This product known as ASTER Global DEM (Tachikawa et al., 2011) was created using data from the Advanced Spaceborne Thermal Emission and Reflection Radiometer (ASTER) image instrument aboard the Terra satellite. The version 1 was released in 2009 and the version 2 in 2011. The latter version employs data collected between 2000 and 2010, covering the earth surface between 83° north and 83° south while its horizontal resolution is around 30 m at the equator. Several authors compared the ASTER in its version 2 to ground control points on various continents and found RMSE of 8 m to 13 m (Gesch et al., 2014; Rexer and Hirt, 2014; Jing et al., 2014; Santillan and Makinano-Santillan, 2016). Due to its lower accuracy than the SRTM, the application of ASTER in flood modelling is sparse, with only few examples of successful utilisation (e.g Tarekegn et al., 2010; Wang et al., 2012).

The latest addition of open-access global DEM is the ALOS World 3D-30m (AW3D30) (Tadono et al., 2016) released in May 2016 by the JAXA. It has been created by using the images of the PRISM panchromatic stereo mapping sensor on board the Advanced Land Observing Satellite (ALOS). This open-access DSM is a resample of a commercial DSM at 5 m. It covers an area roughly between 82° north and 82° south. Due to its novelty, this dataset has seen few use in flood modelling. Table 1 recapitulates the studies that evaluate the AW3D30, and how they differ to the present work. Additionally, we acknowledge that Yamazaki et al. (2017) presented an error-corrected DEM that uses the AW3D30 for filling missing values identified in the SRTM dataset. However, the article does not provide a comparison between those two datasets. In contrast, multiple studies have presented comparisons of the accuracy and differences between the elevation data from SRTM and ASTER. They found that the former performs generally better than the latter (Hirt et al., 2010; Jing et al., 2014; Gesch et al., 2014; Rexer and Hirt, 2014; Jarihani et al., 2015). To the best of our knowledge, the work of Moe et al. (2017) is the only one that evaluates AW3D30 for flood modelling. However that study limits itself to a visual comparison of flood depths between the AW3D30, the SRTM at 3″, and the commercial ALOS DSM at 5 m.

Recognizing the importance of global, open-access DEM for flood modelling (Schumann et al., 2014; Sampson et al., 2016), the objective of this study is twofold. Firstly to present an assessment of the capacity of the AW3D30 for numerical flood modelling and secondly, to compare its performance with other freely available 30 m DEM for model setup (e.g. SRTM and ASTER). For this comparison, the reference to reality is given by the water levels and flood extent maps computed with the same numerical model but using a LiDAR based DTM (5 m of spatial resolution re-sampled to 30 m). The numerical model utilised in this study is a GIS-integrated, open-source dynamic hydrologic and hydraulic model known as Itzï (Courty et al., 2017), which solves a damped partial inertia approximation of the Saint-Venant equations on a regular raster grid (Almeida et al., 2012; Almeida and Bates, 2013). The comparison is carried out in two urban catchments located in Mexico, with contrasting topographic gradients (steep and flat).

This paper is organised as follows, Section 2 introduces the details of the different DEM that are utilised, the study areas and the type of evaluation we perform. Section 3 describes the results we obtained and Section 4 presents a discussion of the implications of results in the context of flood modelling. Finally, Section 5 summarises the main conclusions found in this investigation.

Note of terminology In this paper, we will use the term DSM when referring to data that include vegetation and buildings, and DTM when referring to 'bare-earth' data. DEM is used as an umbrella term that includes both DSM and DTM. The term AW3D30 refers to the ALOS World 3D-30m version 1. We employ the term ASTER to refer to the ASTER GDEM version 2.

Table 1: Published work evaluating the AW3D30.

Reference	Study area	Other elevation references	Type of assessment	Comments
Santillan and Makinano-Santillan (2016)	Northeastern Mindanao, Philippines	ASTER, SRTM 1″, and ground control points.	Vertical accuracy	AW3D30 is more accurate than ASTER and SRTM
Hu et al. (2017)	Hubei Province, China	ASTER, SRTM 1″ and 3″, and 1:50 000 DEM of China	Vertical accuracy	
Grohmann (2018)	Brazil	TanDEM-X 12 m and 30 m, SRTM 1″, and ASTER	Vertical accuracy	AW3D30 has a similar accuracy than TanDEM-X in flat terrains
Moe et al. (2017)	Jakarta, Indonesia	SRTM 1″ and AW3D 5 m and 30 m	Visual comparison of flood depths and extent from numerical modelling	
Present study	Coahuila and Tamaulipas, Mexico	ASTER, SRTM 30 m, and LiDAR	Accuracy of flood modelling compared to LiDAR	

Meanwhile we use the terms SRTM to refer to the Shuttle Radar Topography Mission elevation product, in its 1″ resolution. At the time of writing, only one version was available at that resolution. Finally, we acknowledge that the DEM studied inhere are not actually global, as they leave out the polar regions of the globe. However, they cover most of the inhabited areas of the earth, and the term 'global' to designed them is used by other authors (e.g. Schumann et al., 2014; Hu et al., 2017).

2 Material and methods

2.1 Study areas

Two catchments with important urban areas are selected for the comparison of model results. The urban areas correspond to Saltillo in the state of Coahuila and Reynosa in the state of Tamaulipas, both in the northeastern part of the country. Fig. 1 introduces the geographic location of both cities. The catchments have been defined to cover the majority of the urban areas, while the urban areas are taken from the database of the National Commission for the Knowledge and Use of the Biodiversity of Mexico (CONABIO).

Both catchments represent areas with contrasting terrain physiographies and characteristics. While Saltillo is located in a mountainous region, Reynosa is mainly characterised by flat and low-lying region. Moreover, Table 2 introduces the contrasting characteristics for both cities such as: catchment area, number of raster cells involved in each case, urban area, maximum, minimum and mean slope of the terrain and the corresponding concentration times for both cases. Saltillo represents a larger test case with a quicker rainfall-runoff response in the catchment in comparison to Reynosa.

The urban area of Reynosa includes the municipalities of Reynosa and Río Bravo. The catchment is located at the border with the USA, in the valley of the Río Bravo (also known as Rio Grande in the USA). It includes artificial irrigation structures that initiate at the Anzaldúas dam on the Río Bravo upstream Reynosa. The Anzaldúas canal crosses Reynosa and then passes south of the city of Río Bravo. The Retamal canal branches out of the Anzaldúas canal after Reynosa and circumvent the city of Río Bravo on the north. Those canals are equipped with sluice gates that further modify the natural hydrology of the catchment.

In the case of Saltillo, the urban area includes the municipalities of Ramos Arizpe, Arteaga and Saltillo proper. Most of the built up area lies in a valley on the west of the Sierra Madre Oriental mountain range. The main mountainous area is on the east of the catchment and consists of the Sierra la Martha mountain that culminates at the Cerro San Rafael more than 3700 m above sea level.

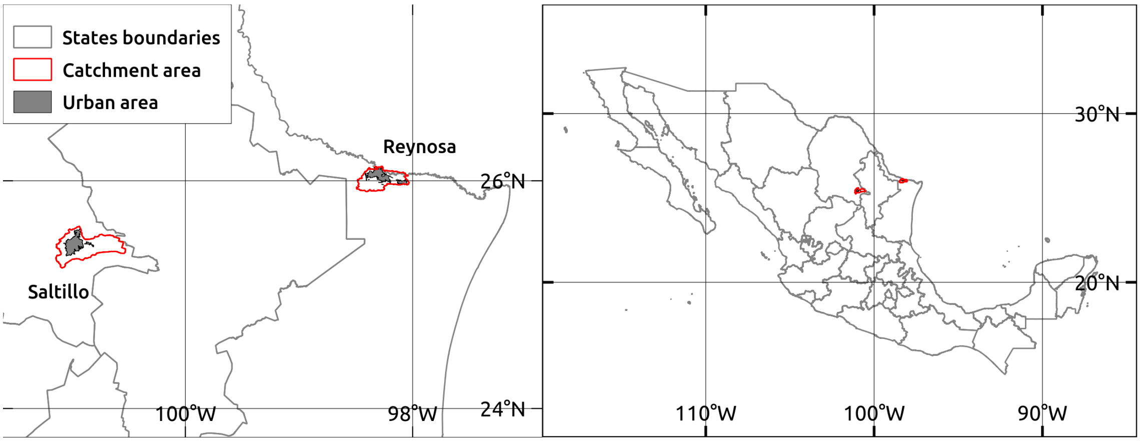

Figure 1: Location of the study areas in Mexico.

Table 2: Informations of the study areas. The population of the urban areas are from National Institute for Statistic and Geography of Mexico (INEGI) (Reynosa 2015, Saltillo 2010), the elevations and slopes are from the LiDAR DTM.

	Reynosa	Saltillo
Population	≈773 000	≈923 000
Catchment area (km^2)	683	1188
#Raster cells	1 273 580	2 745 792
Urban area (km^2)	174.7	229.0
Min. elevation (m)	20	1299
Max. elevation (m)	152	3711
Max. slope (°)	17.9	70.9
Mean slope (°)	0.75	13.75
Median slope (°)	0.5	8.5
t_c (Kirpich, in hours)	19.5	8.5

2.2 Elevation data

Elevation data in the form of DEM have been recognised as a basic piece of information for the accurate representation of topographic controls exerted in both hydrologic (Kenward, 2000) and hydraulic models (Cobby et al., 2001; Meesuk et al., 2015). This is more true in urban environments, where LiDAR derived DTM have been recognised as the best possible source of elevation data (Fewtrell et al., 2008; Gallegos et al., 2009). However, the remote-sensed data compared in this study are DSM. Therefore, in this investigation we use both DSM and DTM derived from LiDAR as references. The DTM serves as a reference to reality while the DSM permits a fairer comparison to global DSM.

LiDAR derived DEM are obtained from the INEGI. In both case studies, two different LiDAR products are utilised with a horizontal resolution of 5 m. The first one corresponds to a DSM, which is based on first echoes with threes, buildings etc., while the second is a DTM where all these features have been removed to obtain a bare-earth model. The INEGI provides only the final raster maps, not the original point cloud, and does not provide details on the procedures used to obtain the said rasters.

For a fair comparison of LiDAR derived DEM against the global DEM of coarser spatial resolution, both LiDAR products are re-sampled to 30 m to compare results at the same spatial resolution. The up-scaling of this information is performed using an arithmetic mean aggregation method.

Table 3 introduces the geographic information related to the different DEM used in this study. All DEM have been projected to a common coordinate system, the Mexico ITRF2008/LCC (EPSG 6372). GRASS GIS (Neteler et al., 2012) and a bilinear interpolation has been used for this task.

Table 3: Geographic information of the raw elevation data. For this study, all data were projected to the same coordinate system and evaluated at 30 m.

Product	Sensing year	Sensor type	Coord. system	Hor. datum	Vert. datum	Hor. res.
LiDAR	2011	Laser	UTM14N	ITRF92	NAVD88	5 m
AW3D30	2006–2011	Optical	lat/long	WGS84	EGM96	$1''$
SRTM	2000	Radar	lat/long	WGS84	EGM96	$1''$
ASTER	2000–2010	Optical	lat/long	WGS84	EGM96	$1''$

With regards to the global DEM we utilise the first version of the SRTM with a resolution of $1''$, while the ASTER corresponds to the second version of the product. Both datasets are downloaded from the United States Geological Survey (USGS) EarthExplorer service. In the case of the AW3D30, we employ the version 1 downloaded from the official JAXA web page. This dataset is an up-scaling of the ALOS World 3D commercial DSM with spatial resolution of 5 m. It should be noted that for this dataset, two versions of the data are distributed, which depend on the aggregation method used during the re-sampling: mean or median. In this investigation, we use the data obtained by the arithmetic mean method. In both catchment, this dataset was checked for voids and invalid data using the mask layer distributed alongside the data. In Saltillo, the area is completely covered with valid data. In the case of Reynosa, the dataset presents a 0.1 % of voids and 0.57 % of pixels identified by JAXA as land water and 'low correlation'. Those pixels were filled using an interpolation technique based on the regularised spline with tension (Mitášová and Mitáš, 1993).

We acknowledge that raw DEM, and especially remote-sensed DSM need to be preprocessed in order to improve the results of hydrologic and hydraulic modelling. Such preprocessing techniques could range from vegetation smoothing and stream burning (e.g. Jarihani et al., 2015) to compensating instruments errors (e.g. Yamazaki et al., 2017). Additionally, the use of unconditioned space-borne DSM, although allegedly not optimum, is not totally uncommon(e.g. Sanders, 2007; Castro et al., 2016; Busaman et al., 2015; LeFavour and Alsdorf, 2005; Huggel et al., 2008). It is therefore worthwhile to assess the performance of raw dataset in order to 1) give an indication to the practitioners that will use them as is, and 2) as an indication of there there potential after conditioning.

2.3 Comparison of slope and aspect

As seen in Table 3 the selected DEM have different vertical reference systems. In Mexico, INEGI maintains a network of land survey benchmarks in yet another vertical datum (NAVD29). This complicates the comparison of absolute altitudes between DEM. Furthermore, we consider that the absolute altitude is a poor indicator of a DEM's capacity for flood simulations. For this reason, we decided not to perform a comparison of altitude. Instead, the comparison of the relative altitude difference between cells (i.e. slope and aspect) is implemented. This characteristic is of better help when the evaluation of a DEM for flood modelling is sought. Indeed, most of the physically-based flood models, including the one used in this paper, rely on the altitude differences between two raster cells to calculate the flow. Therefore, the absolute accuracy of the elevation above the mean sea level is of little help to evaluate the quality of a DEM for flood modelling.

The LiDAR-derived DTM are used as reference, as the *bare-earth* model is considered the best suited for flood modelling (Sampson et al., 2016). In the case of very smooth slopes and to prevent errors in aspect calculation, the minimum slope to undertake this mathematical operation is set to 0.02°. Otherwise, the aspect is not evaluated. The aspect map represents the direction which the slope is facing, in degrees counter-clockwise from east. The angle error $\Delta\phi$ is calculated using Eq. 1, where ϕ_1 and ϕ_2 are the compared angles.

$$\epsilon = |(\phi_1 - \phi_2)| \tag{1a}$$

$$\Delta\phi = 180 - |\epsilon - 180| \tag{1b}$$

2.4 Numerical model

The numerical tool utilised in this investigation corresponds to a GIS-integrated, open-source dynamic hydrologic and hydraulic model known as Itzï (Courty et al., 2017). This model solves a damped partial inertia approximation of the Saint-Venant equations on a regular raster grid (Almeida et al., 2012; Almeida and Bates, 2013). The time-step duration Δt is calculated at each time-step using Eq. 2, where h_{max} is the maximum water depth within the domain, g the acceleration due to the gravity and α an adjustment factor.

$$\Delta t = \alpha \frac{\min\{\Delta x, \Delta y\}}{\sqrt{g \times h_{max}}} \tag{2}$$

The flow between cells q is calculated with Eq. 3, where subscripts i and t denotes space and time indices, S the hydraulic slope and θ an inertia weighting factor. The flow depth h_f is the difference between the highest water surface elevation y and the highest terrain elevation z. It is used as an approximation of the hydraulic radius.

$$q_{i+1/2}^{t+\Delta t} = \frac{\left(\theta q_{i+1/2}^{t} + (1-\theta)\dfrac{q_{i-1/2}^{t} + q_{i+3/2}^{t}}{2}\right) + g h_f \Delta t S}{1 + g \Delta t n^2 ||q_{i+1/2}^{t}|| / {h_f}^{7/3}} \tag{3}$$

The water depth at each cell centre is calculated using Eq. 4. It is the sum of the current depth h^t, the external factors h_{ext}^t (rainfall, infiltration, drainage etc.) and the flows passing through the four faces of each cell.

$$h^{t+\Delta t} = h^t + h_{ext}^t + \frac{\sum^4 Q_{i,j}^t}{\Delta x \Delta y} \times \Delta t \tag{4}$$

2.5 Model set-up

In order to evaluate solely the influence of the DEM on the model results, we define a synthetic rainfall storm event uniform in space and constant in time at $10\,\mathrm{mm\,h^{-1}}$. Moreover, the friction is also considered spatially uniform and is set to a Manning's n coefficient of $0.04\,\mathrm{s\,m^{-1/3}}$. The infiltration and evapotranspiration are neglected. Additionally, in the case of the city of Reynosa, there is a clear influence of the upstream flow from the Río Bravo, which for the purposes of this investigation is neglected. The objective of using an over-simplify synthetic set-up is to isolate as much as possible the influence of the elevation data on the numerical results. While using historical events would have the advantage of providing a reference for the 'right' results, one must consider the uncertainty related to observations and that different events could trigger different responses from the catchment, with varying influence from the DEM. Table 4 introduces a summary of the simulation parameters utilised in both cases (Reynosa and Saltillo).

In both catchments, downstream boundary conditions are set to allow the outflow of water from the numerical domain. Moreover, the discharge of water flowing through these outflow boundaries is recorded. The simulation time is set to 48 h, which is considered sufficient to allow flow stabilisation in both cases, as this is longer than the estimated concentration times (See Table 2).

Table 4: Simulation parameters

Parameter	Value
α^1	0.5
Δt_{max} (s)^2	1.0
θ^3	0.8
Manning's n ($\mathrm{s\,m^{-1/3}}$)	0.04
Rainfall (mm/h)	10.0

[1] time-step adjusting factor.
[2] maximum time-step.
[3] inertia weighting coefficient.

Numerical results with regards to water depths and flood extents are reported in each case. For clarity in the comparison of model results between runs, a numerical threshold to define a flooded element is set to 20 cm. We use the Critical Success Index (CSI) to quantitatively determine the model skill with regards to flood extent area. This score is commonly used in hydrology (e.g. Horritt and Bates, 2002; Cook and Merwade, 2009) and is defined as CSI $= \frac{\text{hits}}{\text{hits}+\text{misses}+\text{false alarms}}$, following the values determined by a contingency table (see Table 5). The reference to reality is ascribed to those numerical results obtained by using the LiDAR-based DTM.

Table 5: Contingency table used to calculate the CSI.

		Observed	
		Flooded	Not flooded
Computed	Flooded	hits	false alarms
	Not flooded	misses	correct negatives

3 Results

3.1 Comparison of slope and aspect

Figure 2 displays for both cities, the Mean Absolute Error (MAE) in slope and aspect resulting from the comparison of these variables derived for each DEM against those calculated using the

LiDAR DTM as a reference. It is shown, that all tested DEM have clear differences when compared against the LiDAR DTM. In this Figure, bars represent the size of the error where a smaller bar indicates a better performance.

Notably in Saltillo, where the catchment is characterised by steeper gradients, the slope errors are greater than those registered in Reynosa (region with smoother slopes). In contrast, the aspect errors in the city with stepper gradients (Saltillo) are notably lower than those reported in the smother gradients region (Reynosa). This may be ascribed to the steeper slopes in the former that might prevent changes in aspect due to absolute altitude variation.

Naturally, in these results the LiDAR-derived DSM is the dataset best performance (e.g. smaller errors). Furthermore, the SRTM reports a better accuracy than that reported by the ASTER, which incidentally is the dataset with poorest performance in both cases.

Results estimated in both catchments for the AW3D30, show a better performance of this dataset than that reported by the SRTM. Noticeably, in the steeper gradient region (Saltillo) the MAE of slope reported for the AW3D30, is nearly two times smaller than that registered for the SRTM. Whereas in the region with smoother slopes (Reynosa), results of MAE in slope show similar performance between both the AW3D30 and the SRTM, with a very small advantage of the latter.

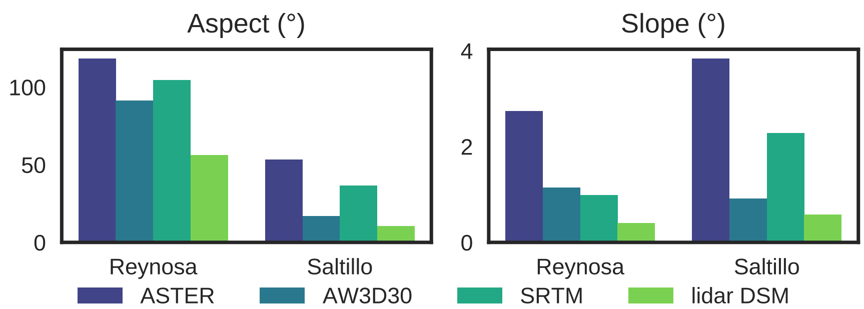

Figure 2: Mean Absdolute Error in slope and aspect of each DEM compared to the LiDAR DTM. Lower is better.

3.2 Inundation modelling

3.2.1 Qualitative analysis of water depth maps

In both cities, a qualitative analysis of the numerical results was deemed necessary, as there were clear differences between results in the numerical runs using the selected DEM.

This was especially true in the results of the region with smoother slope (Reynosa), which are illustrated in Fig. 3. Different panels in this Figure show flood maps corresponding to the water depths registered at the end of the simulation time. Clearly and naturally, the less noisy output is obtained with the LiDAR derived DTM, which is our reference to reality. The smoothness of the solution degrades with each product in the following order: the LiDAR derived DSM, the AW3D30 and the SRTM. Numerical results using the ASTER, provide a very noisy picture of this variable, indicating the little use of this dataset for this region as no clear flow path is distinguishable. These results are in accordance to those obtained in the comparison of slope and aspect.

Figure 4 introduces the same flood maps but determined at the end of the simulation time for the city of Saltillo, which is a region characterised by steeper slopes. In this case, similar results are obtained. However, in the case of the ASTER the outcome the flow paths appear more clearly.

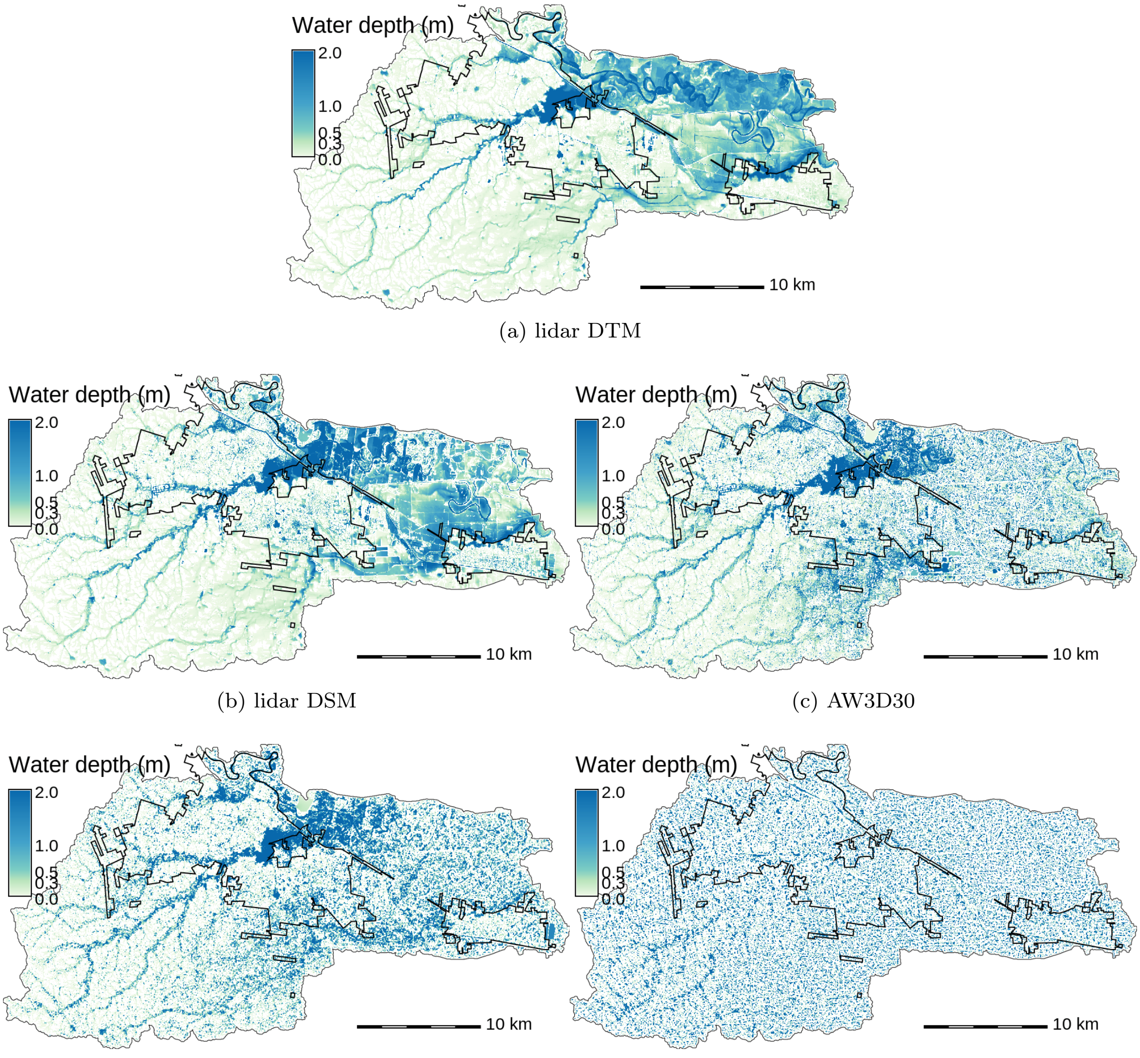

(a) lidar DTM

(b) lidar DSM

(c) AW3D30

(d) SRTM

(e) ASTER

Figure 3: Water levels at the end of the simulations in the flat catchment of Reynosa.

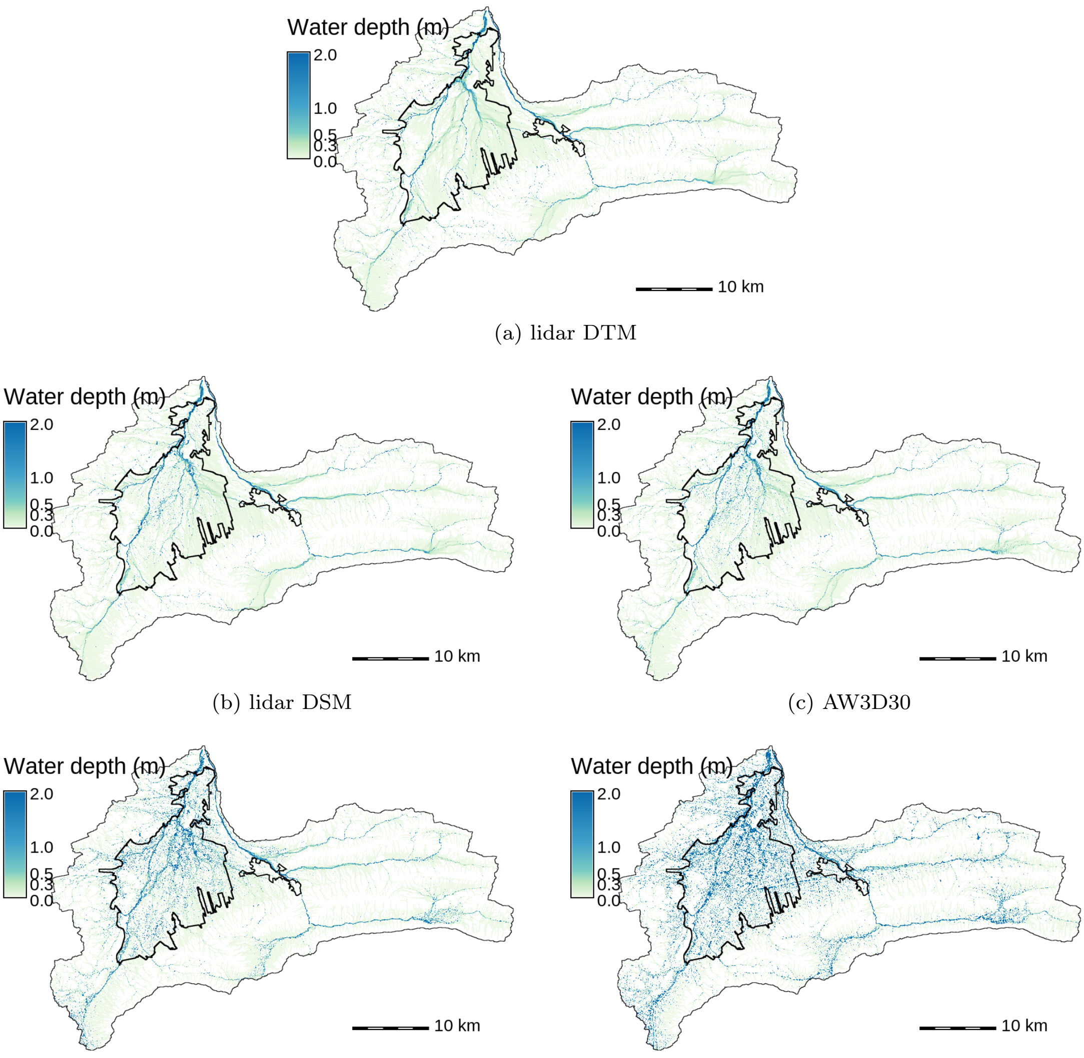

(a) lidar DTM

(b) lidar DSM

(c) AW3D30

(d) SRTM

(e) ASTER

Figure 4: Water levels at the end of the simulations in the hilly catchment of Saltillo.

3.2.2 Time evolution of water volume within the domain

When a permanent rainfall occurs on a given DEM, the water volume in the domain and the outflow will eventually stabilise. However, both the time it takes to reach this equilibrium state and the shape of the curve give us indications about the level noise of the evaluated DEM and its impact on the hydraulic simulation.

Top panels of Figure 5 represent for both cases (flat - left and steep - right gradient) the time evolution of water volume within the domain, while bottom panels introduce the time series of the outflow recorded exiting the domain in both areas. It is acknowledged that when the outflow and the domain volume stabilise, the numerical run has reached an equilibrium state due to the permanent forcing conditions. For this exercise, we consider that the model stabilise when the net addition to the domain volume falls under $1\,\mathrm{hm}^3\,\mathrm{h}^{-1}$. Moreover, bottom panels in Fig. 5 allows us to estimate the time at which the flood wave reaches the outlet of the catchment. It is clear that in the catchment with steeper gradient (right bottom panel), the propagation of the flood wave is quicker than that observed in the lower gradient case with a value smaller than 6 hours.

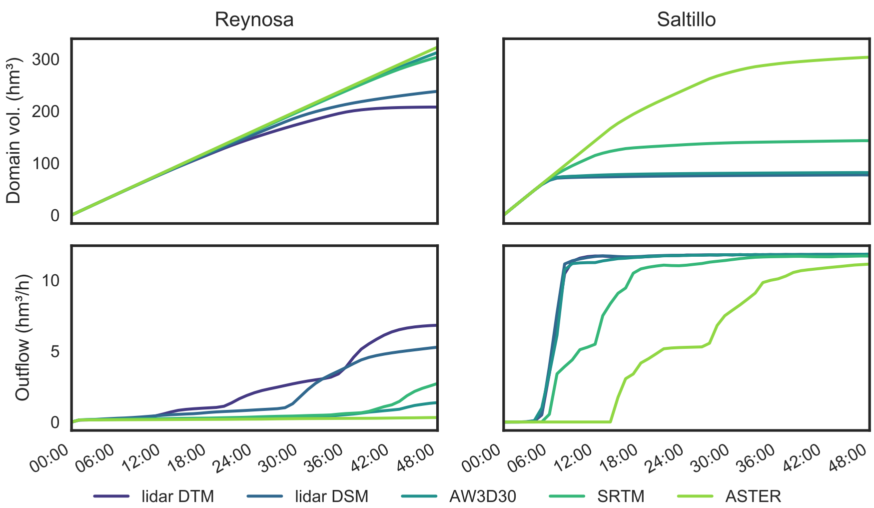

Figure 5: Time evolution of the water volume and outflow in the two observed computational domains. The time to equilibrium and curve shape are indicators of the effect of the DEM noise on the hydraulic simulation.

Remarkably, in the case of the region with steeper slopes, Saltillo, the two LiDAR derived DEM and the AW3D30 show a very similar behaviour of the flood wave, with arrival times between 5 to 6 hours and a stabilisation time between 8 to 9 hours. In contrast, results for the SRTM and the ASTER show a clear deviation in the time evolution of both variables (volume and outflow), which casts some doubt in their adequacy for flood modelling in such study region. Moreover, the registered flood wave propagation times to the outflow point using LiDAR and AW3D30 are in accordance with the concentration time (8.5 h) estimated through the Kirpich formula (See Table 2).

In the case of the numerical results using the SRTM, the first flood wave arrives one hour later but does not stabilise until 19 h. This fact produces a flood volume almost twice as big as that registered in the numerical results using the LiDAR DTM ($77\,\mathrm{hm}^3$ versus $143\,\mathrm{hm}^3$). Similarly, numerical results obtained with the ASTER DSM produce a propagation time of 15 h and a stabilisation time of 43 h. In turn, this yields a flood volume that is 4 times larger than that obtained in the numerical run using the LiDAR derived DTM ($303\,\mathrm{hm}^3$ versus $77\,\mathrm{hm}^3$).

The results obtained in the region with lower gradients indicate that for the simulation with the LiDAR derived DTM, the flood wave requires a larger time before reaching equilibrium (41 h). Indeed, none of the simulations ran with the selected global DEM reaches the equilibrium. The numerical results using the AW3D30 and the SRTM show the start of a significant outflow around 38 h and 40 h, respectively. Lastly, simulation results obtained with the ASTER show no hydraulic connectivity, as the outlfow after 48 hours is only $0.3\,\mathrm{hm}^3\,\mathrm{h}^{-1}$).

3.2.3 Comparison of simulated water depths

A key variable in the validation of model results, when simulating floods is the total water depth. This variable is important to determine the level of damage that may be ascribed to a flood event, as it is utilised in the definition of flood hazard levels within a city or catchment.

Therefore, numerical results of this variable are also compared in both cases. Once again, reference values are determined through the results of the simulation using the LiDAR based DTM.

The results of this exercise are presented in Fig. 6, where left panel shows the results for the smooth gradient region (Reynosa) and the right panel introduces the results for the region with steep gradient (Saltillo). Results in both regions are classified in relation to the spatial location of the point of analysis (e.g. non-urban, urban and whole). This is done in order to analyse further whether there is a difference in the performance in the model in urban areas of the region.

As expected, in both selected cities, the DEM with the best performance (smaller error), is given by the LiDAR derived DSM. Notably, the second best dataset is the AW3D30, with a mean absolute error in the water depths that is in the order of that registered to the LiDAR DSM in the steep gradient case (Saltillo). Additionally, in this catchment, the errors in all DEM are proved to be higher in the urban area than outside of it. This could be explained by two factors. First, the city is situated in an area of lower slopes, compared to the mountain range that comprises a large part of the non-urban area. This means that the DEM errors could be compensated by the higher slopes and hence are less noticeable. Second, it is known that urban areas are challenging for surface models, mainly due to the noise introduced by the sensors echo on the buildings.

In contrast, in the smooth gradient city (Reynosa), the skill of the AW3D30 is not as good as that observed with the LiDAR derived DSM. Indeed, errors registered by the AW3D30 in this case, are in the same order of magnitude as those registered with the SRTM. Conversely, there no significant differences in the levels of errors between urban and non-urban areas in Reynosa. This could be due to the higher percentage of urbanised area (26 % versus 19 %, see Table 2) and that there is no strong changes of slopes between the non-urban and urban areas.

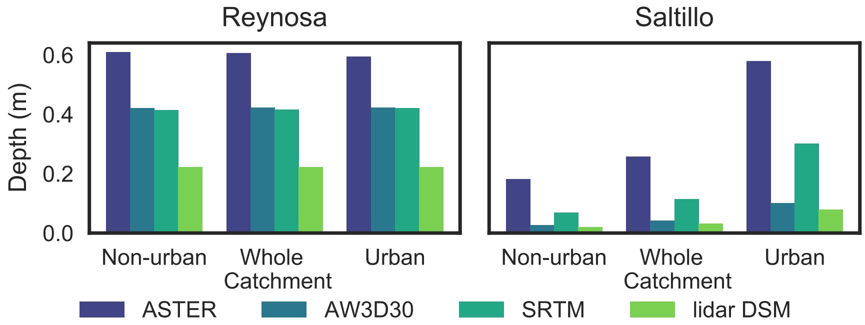

Figure 6: Mean Absolute Error in maximum water depth for each DEM compared to the LiDAR DTM. Only values above 20cm are taken into account. Lower is better.

3.2.4 Comparison of flood extent

Finally, the last numerical result that is incorporated in the discussion is that related to the affected area by the flood in each numerical run. Therefore, an evaluation of the differences in flood extent maps is carried out. For this, we compute the CSI (Stanski et al., 1989) determined by comparing the numerical result of each model run (AW3D30, SRTM, ASTER and LiDAR DSM) and city (Reynosa and Saltillo) against that obtained with the LiDAR derived DTM.

Figure 7 presents for both selected cities, the CSI values for each numerical run using the different DEM. In accordance to the results related to water depths, the LiDAR derived DSM presents the best skill of all DEM analysed, while the ASTER has very low values of CSI in both cases, indicating the poor suitability for its utilisation 'as is' in flood modelling studies.

Right panel in Figure 7 summarises the results for the steep gradient region (Saltillo), where the AW3D30 is proven to be the best dataset when comparing flood extent results against the other open global DEM. Computed CSI values range between 0.40 and 0.61 and are within 0.1 of those obtained with the LiDAR derived DSM. In this catchment, it is noticeable that the CSI is reduced when moving from the non-urban area to the urban area, which is coherent with the results obtained when observing the water depth (see Fig. 6).

On the other hand, in the smooth gradient region of the city of Reynosa, numerical results indicate a degradation of the skill when using the AW3D30. Indeed, the CSI values computed with this DSM are again in accordance to those computed using the results of the SRTM. This may indicate that in regions with smooth gradients the performance of the AW3D30 is similar to that registered using the SRTM.

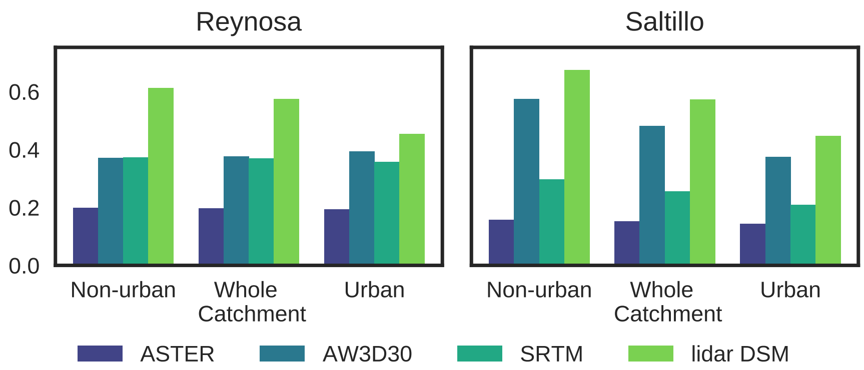

Figure 7: Critical Success Index calculated against the flood extent obtained with the LiDAR DTM. A cell is considered flooded when the water depth is above 20 cm. Perfect score is 1.

4 Discussion

Our results show that the AW3D30 is a welcome addition to the body of open-access global DEM. Notably, in hilly areas characterised by steep gradients, the AW3D30 displays a clear improvement over the SRTM. Its performances in computer flood modelling approach those obtained with a LiDAR DSM at the same horizontal resolution. This advantage is reduced in smooth gradient areas, but in this case, numerical results obtained with the AW3D30 are at least as good as those registered using the SRTM.

Two reasons could explain those results: the type of sensor and the original resolution of the product. The AW3D30 is obtain by photogrammetry from optical images (i.e. passive sensor), while the SRTM is created via InSAR (i.e. active sensor). An active sensor might penetrate more the vegetation than a passive sensor, and therefore results in a DEM that is closer to the terrain. Whereas a DEM created from optical imagery, like AW3D30, will always represent the top of the vegetation. This could explain the less impressive results of the AW3D30 in the flat catchment of Reynosa, where the relative influence of vegetation is higher. In the case of the AW3D30, this perceived weakness is compensated by the higher native resolution of the data. Indeed, the AW3D30 is a resampling of a 5 m commercial DEM, while the SRTM and ASTER are created at a resolution of 30 m. The resulting practical resolution of the AW3D30 is much higher than the other products.

However, the accuracy of global DEM depends largely on the number of passes of the spacecraft above a given region and the usability of the collected data, for example due to cloud cover. The higher the number of passes and the lower the cloud cover, the higher the quality. There is indeed a spatial variability in the quality and availability of the same product. The present work describes results obtained in the north-east of Mexico and thus might not be representative of the accuracy of the studied DEM in all regions of the world. Hence, it would be valuable to perform such an evaluation of the AW3D30 in other parts of the planet. Moreover, herein we evaluate the version of the AW3D30 obtained through the arithmetic mean aggregation of the commercial AW3D at 5 m. Some more work is needed to evaluate the differences that may occur by using the version obtained from the median aggregation. Finally, the AW3D30 is still a DSM, and therefore it includes noise and bias due to tree cover and buildings.

We see that AW3D30 does not address all the issues reproached to open-access global DEM (Schumann et al., 2014; Simpson et al., 2015; Sampson et al., 2016). Nevertheless, it is a clear improvement compared to the SRTM, especially in areas of higher slopes. When possible, this DSM may replace the SRTM as a base for hydraulic conditioning that would further improve its performance when used in computer flood modelling, like it has been done with other products (e.g. Lehner et al., 2008; Jarihani et al., 2015; O'Loughlin et al., 2016; Yamazaki et al., 2017). This would pave the way to an increase in accuracy of global flood models (Trigg et al., 2016) and in risk mapping in data-scarce countries.

5 Conclusion

Elevation datasets are acknowledged to play a significant role in hydrologic and hydraulic modelling of flood events. Moreover, flood inundation maps represent a key piece of information in preventing and reducing losses, as they enable the dissemination of flood risk to the society and decision makers (Rodríguez-Rincón et al., 2015). However, DEM of high resolution and accuracy are not available in all regions of the world.

In this paper we evaluated the suitability of the AW3D30 for computer flood modelling. We compared it with DSM and DTM obtained from aerial LiDAR and to other open-access global DSM at the same resolution of $1''$: the SRTM and the ASTER. In every observed metrics, the ASTER is the worst performer of all global DSM. In terrains with higher slopes, the AW3D30 performs better than the SRTM in every metrics, in both urban and rural areas. Notably, the performance of the AW3D30 is comparable to the resampled DSM obtained by LiDAR. In lower slopes, the improvement over the SRTM is still present, although at a smaller scale.

Similar evaluation needs to be done in other part of the world to confirm the encouraging proposition of the AW3D30. Additional investigation is needed to assess the possible differences between the median and mean versions of the product. Finally, further work might focus on the production of a hydrologically conditioned elevation model based on the AW3D30.

References

Almeida, G. A. M. de and P. D. Bates (2013). 'Applicability of the local inertial approximation of the shallow water equations to flood modeling'. In: *Water Resources Research* 49.8, pp. 4833–4844. ISSN: 00431397. DOI: 10.1002/wrcr.20366.

Almeida, G. A. M. de, P. D. Bates, J. E. Freer, and M. Souvignet (2012). 'Improving the stability of a simple formulation of the shallow water equations for 2-D flood modeling'. In: *Water Resources Research* 48.5, pp. 1–14. ISSN: 00431397. DOI: 10.1029/2011WR011570.

Bates, P. D. (2004). 'Remote sensing and flood inundation modelling'. In: *Hydrological Processes* 18.13, pp. 2593–2597. ISSN: 0885-6087. DOI: 10.1002/hyp.5649. URL: http://doi.wiley.com/10.1002/hyp.5649.

Busaman, A., K. Mekchay, S. Siripant, and S. Chuai-Aree (2015). 'Diffusion modelling on a dynamically adaptive tree grid for rainfall overland flow simulation'. In: *ScienceAsia* 41, pp. 414–422. DOI: 10.2306/scienceasia1513-1874.2015.41.414. URL: http://scienceasia.org/2015.41.n6/scias41%7B%5C_%7D414.pdf.

Castro, L., B. Fernandez, F. Suarez, and T. Maas (2016). 'Integrated system for streamflow forecast in mountain basins for hydropower operation'. In: *12th International Conference on Hydroinformatics.*

Cobby, D. M., D. C. Mason, and I. J. Davenport (2001). 'Image processing of airborne scanning laser altimetry data for improved river flood modelling'. In: *ISPRS Journal of Photogrammetry and Remote Sensing* 56.2, pp. 121–138. ISSN: 09242716. DOI: 10.1016/S0924-2716(01)00039-9.

Cook, A. and V. Merwade (2009). 'Effect of topographic data, geometric configuration and modeling approach on flood inundation mapping'. In: *Journal of Hydrology* 377.1-2, pp. 131–142. ISSN: 00221694. DOI: 10.1016/j.jhydrol.2009.08.015. URL: http://linkinghub.elsevier.com/retrieve/pii/S0022169409004909.

Courty, L. G., A. Pedrozo-Acuña, and P. D. Bates (2017). 'Itzï (version 17.1): an open-source, distributed GIS model for dynamic flood simulation'. In: *Geoscientific Model Development* 10.4, pp. 1835–1847. DOI: 10.5194/gmd-10-1835-2017. URL: http://www.geosci-model-dev.net/10/1835/2017/.

Di Baldassarre, G. (2012). 'Data sources'. In: *Floods in a Changing Climate: Inundation Modelling.* Cambridge: Cambridge University Press, pp. 33–42. DOI: 10.1017/CBO9781139088411.008. URL: http://ebooks.cambridge.org/ref/id/CBO9781139088411A013.

Farr, T. G., P. A. Rosen, E. Caro, R. Crippen, R. Duren, S. Hensley, M. Kobrick, M. Paller, E. Rodriguez, L. Roth, D. Seal, S. Shaffer, J. Shimada, J. Umland, M. Werner, M. Oskin, D. Burbank, and D. E. Alsdorf (2007). 'The Shuttle Radar Topography Mission'. In: *Reviews of*

Geophysics 45.2, RG2004. ISSN: 8755-1209. DOI: 10.1029/2005RG000183. URL: http://doi.wiley.com/10.1029/2005RG000183.

Fewtrell, T. J., P. D. Bates, M. S. Horritt, and N. M. Hunter (2008). 'Evaluating the effect of scale in flood inundation modelling in urban environments'. In: *Hydrological Processes* 22.26, pp. 5107–5118. ISSN: 08856087. DOI: 10.1002/hyp.7148. URL: http://doi.wiley.com/10.1002/hyp.7148.

Gallegos, H. A., J. E. Schubert, and B. F. Sanders (2009). 'Two-dimensional, high-resolution modeling of urban dam-break flooding: A case study of Baldwin Hills, California'. In: *Advances in Water Resources* 32.8, pp. 1323–1335. ISSN: 03091708. DOI: 10.1016/j.advwatres.2009.05.008.

Gesch, D. B., M. J. Oimoen, and G. A. Evans (2014). *Accuracy assessment of the U.S. Geological Survey National Elevation Dataset, and comparison with other large-area elevation datasets: SRTM and ASTER.* Tech. rep. DOI: 10.3133/OFR20141008. URL: https://pubs.er.usgs.gov/publication/ofr20141008.

Grohmann, C. H. (2018). 'Evaluation of TanDEM-X DEMs on selected Brazilian sites: comparison with SRTM, ASTER GDEM and ALOS AW3D30'. In: arXiv: 1709.05016v2. URL: http://arxiv.org/abs/1709.05016v2.

Hallegatte, S., C. Green, R. J. Nicholls, and J. Corfee-Morlot (2013). 'Future flood losses in major coastal cities'. In: *Nature climate change* 3.9, pp. 802–806. DOI: 10.1038/nclimate1979.

Hirabayashi, Y., R. Mahendran, S. Koirala, L. Konoshima, D. Yamazaki, S. Watanabe, H. Kim, and S. Kanae (2013). 'Global flood risk under climate change'. In: *Nature Climate Change* 3.9, pp. 816–821. ISSN: 1758-678X. DOI: 10.1038/nclimate1911. URL: http://www.nature.com/doifinder/10.1038/nclimate1911.

Hirt, C., M. S. Filmer, and W. E. Featherstone (2010). 'Comparison and validation of the recent freely available ASTER-GDEM ver1, SRTM ver4.1 and GEODATA DEM-9S ver3 digital elevation models over Australia'. In: *Australian Journal of Earth Sciences* 57.3, pp. 337–347. ISSN: 0812-0099. DOI: 10.1080/08120091003677553. URL: http://www.tandfonline.com/doi/abs/10.1080/08120091003677553.

Hodgson, M. E. and P. Bresnahan (2004). 'Accuracy of Airborne Lidar-Derived Elevation'. In: *Photogrammetric Engineering & Remote Sensing* 3, pp. 331–339. ISSN: 00991112. DOI: 10.14358/PERS.70.3.331.

Horritt, M. S. and P. D. Bates (2001). 'Effects of spatial resolution on a raster based model of flood flow'. In: *Journal of Hydrology* 253.1-4, pp. 239–249. ISSN: 00221694. DOI: 10.1016/S0022-1694(01)00490-5. URL: http://linkinghub.elsevier.com/retrieve/pii/S0022169401004905.

Horritt, M. S. and P. D. Bates (2002). 'Evaluation of 1D and 2D numerical models for predicting river flood inundation'. In: *Journal of Hydrology* 268.1-4, pp. 87–99. ISSN: 00221694. DOI: 10.1016/S0022-1694(02)00121-X. URL: http://www.sciencedirect.com/science/article/pii/S002216940200121X.

Hou, A. Y., R. K. Kakar, S. Neeck, A. A. Azarbarzin, C. D. Kummerow, M. Kojima, R. Oki, K. Nakamura, and T. Iguchi (2014). 'The Global Precipitation Measurement Mission'. EN. In: *Bulletin of the American Meteorological Society* 95.5, pp. 701–722. ISSN: 0003-0007. DOI: 10.1175/BAMS-D-13-00164.1. URL: http://journals.ametsoc.org/doi/abs/10.1175/BAMS-D-13-00164.1.

Hu, Z., J. Peng, Y. Hou, and J. Shan (2017). 'Evaluation of Recently Released Open Global Digital Elevation Models of Hubei, China'. In: *Remote Sensing* 9.3, p. 262. ISSN: 2072-4292. DOI: 10.3390/rs9030262. URL: http://www.mdpi.com/2072-4292/9/3/262.

Huggel, C., D. Schneider, P. J. Miranda, H. Delgado Granados, and A. Kääb (2008). 'Evaluation of ASTER and SRTM DEM data for lahar modeling: A case study on lahars from Popocatépetl Volcano, Mexico'. In: *Journal of Volcanology and Geothermal Research* 170.1-2, pp. 99–110. ISSN: 03770273. DOI: 10.1016/j.jvolgeores.2007.09.005. URL: http://linkinghub.elsevier.com/retrieve/pii/S0377027307002909.

IFRC (2016). *World Disasters Report 2016. Resilience : saving lives today, investing for tomorrow*, p. 282. ISBN: 9789291392407. URL: http://www.ifrc.org/en/publications-and-reports/world-disasters-report/world-disasters-report/.

Jarihani, A. A., J. N. Callow, T. R. McVicar, T. G. Van Niel, and J. R. Larsen (2015). 'Satellite-derived Digital Elevation Model (DEM) selection, preparation and correction for hydrodynamic modelling in large, low-gradient and data-sparse catchments'. In: *Journal of Hydrology* 524, pp. 489–506. ISSN: 00221694. DOI: 10.1016/j.jhydrol.2015.02.049.

Jing, C., A. Shortridge, S. Lin, and J. Wu (2014). 'Comparison and validation of SRTM and ASTER GDEM for a subtropical landscape in Southeastern China'. In: *International Journal of Digital Earth* 7.12, pp. 969–992. ISSN: 1753-8947. DOI: 10.1080/17538947.2013.807307. URL: http://www.tandfonline.com/doi/abs/10.1080/17538947.2013.807307.

Kenward, T. (2000). 'Effects of Digital Elevation Model Accuracy on Hydrologic Predictions'. In: *Remote Sensing of Environment* 74.3, pp. 432–444. ISSN: 00344257. DOI: 10.1016/S0034-4257(00)00136-X.

LeFavour, G. and D. E. Alsdorf (2005). 'Water slope and discharge in the Amazon River estimated using the shuttle radar topography mission digital elevation model'. In: *Geophysical Research Letters* 32.17. ISSN: 00948276. DOI: 10.1029/2005GL023836. URL: http://doi.wiley.com/10.1029/2005GL023836.

Lehner, B., K. Verdin, and A. Jarvis (2008). ‘New Global Hydrography Derived From Spaceborne Elevation Data’. In: *Eos, Transactions American Geophysical Union* 89.10, p. 93. ISSN: 0096-3941. DOI: 10.1029/2008EO100001. URL: http://doi.wiley.com/10.1029/2008EO100001.

Marks, K. and P. D. Bates (2000). ‘Integration of high-resolution topographic data with floodplain flow models’. In: *Hydrological Processes* 14.11-12, pp. 2109–2122. ISSN: 0885-6087. DOI: {10.1002/1099-1085(20000815/30)14:11/12<2109::AID-HYP58>3.0.CO;2-1}.

Meesuk, V., Z. Vojinović, A. E. Mynett, and A. F. B. Abdullah (2015). ‘Urban flood modelling combining top-view LiDAR data with ground-view SfM observations’. In: *Advances in Water Resources* 75, pp. 105–117. ISSN: 03091708. DOI: 10.1016/j.advwatres.2014.11.008.

Mitášová, H. and L. Mitáš (1993). ‘Interpolation by regularized spline with tension: I. Theory and implementation’. In: *Mathematical Geology* 25.6, pp. 641–655. ISSN: 08828121. DOI: 10.1007/BF00893171.

Moe, I. R., S. Kure, N. F. Januriyadi, S. Kazama, K. Udo, and S. Koshimura (2017). ‘Development of a Rainfall Runoff and Flood Inundation Model for Jakarta, Indonesia, and Its Sensitivity Analysis of Datasets to Flood Inundation’. In: *World Environmental and Water Resources Congress 2017*. Reston, VA: American Society of Civil Engineers, pp. 104–116. ISBN: 9780784480601. DOI: 10.1061/9780784480601.010. URL: http://ascelibrary.org/doi/10.1061/9780784480601.010.

Neteler, M., M. H. Bowman, M. Landa, and M. Metz (2012). ‘GRASS GIS: A multi-purpose open source GIS’. In: *Environmental Modelling & Software* 31, pp. 124–130.

O’Loughlin, F. E., R. Paiva, M. Durand, D. E. Alsdorf, and P. D. Bates (2016). ‘A multi-sensor approach towards a global vegetation corrected SRTM DEM product’. In: *Remote Sensing of Environment* 182, pp. 49–59. ISSN: 00344257. DOI: 10.1016/j.rse.2016.04.018. URL: http://linkinghub.elsevier.com/retrieve/pii/S0034425716301821.

Pedrozo-Acuña, A., I. Mariño-Tapia, C. Enriquez, G. Medellín Mayoral, and F. J. González Villareal (2012). ‘Evaluation of inundation areas resulting from the diversion of an extreme discharge towards the sea: case study in Tabasco, Mexico’. In: *Hydrological Processes* 26.5, pp. 687–704. ISSN: 08856087. DOI: 10.1002/hyp.8175. URL: http://doi.wiley.com/10.1002/hyp.8175.

Pedrozo-Acuña, A., J. P. Rodríguez-Rincón, M. Arganis-Juárez, R. Domínguez-Mora, and F. J. González Villareal (2015). ‘Estimation of probabilistic flood inundation maps for an extreme event: Pánuco River, México’. In: *Journal of Flood Risk Management* 8.2, pp. 177–192. ISSN: 1753318X. DOI: 10.1111/jfr3.12067. URL: http://doi.wiley.com/10.1111/jfr3.12067.

Rexer, M. and C. Hirt (2014). ‘Comparison of free high resolution digital elevation data sets (ASTER GDEM2, SRTM v2.1/v4.1) and validation against accurate heights from the Australian National Gravity Database'. In: *Australian Journal of Earth Sciences* 61.2, pp. 213–226. ISSN: 0812-0099. DOI: 10.1080/08120099.2014.884983. URL: http://www.tandfonline.com/doi/abs/10.1080/08120099.2014.884983.

Rodríguez-Rincón, J. P., A. Pedrozo-Acuña, and J. A. Breña-Naranjo (2015). 'Propagation of hydro-meteorological uncertainty in a model cascade framework to inundation prediction'. In: *Hydrology and Earth System Sciences* 19.7, pp. 2981–2998. ISSN: 1607-7938. DOI: 10.5194/hess-19-2981-2015. URL: http://www.hydrol-earth-syst-sci.net/19/2981/2015/.

Sampson, C. C., A. M. Smith, P. D. Bates, J. C. Neal, L. Alfieri, and J. E. Freer (2015). 'A high-resolution global flood hazard model'. In: *Water Resources Research* 51.9, pp. 7358–7381. ISSN: 00431397. DOI: 10.1002/2015WR016954. URL: http://doi.wiley.com/10.1002/2015WR016954.

Sampson, C. C., A. M. Smith, P. D. Bates, J. C. Neal, and M. A. Trigg (2016). 'Perspectives on Open Access High Resolution Digital Elevation Models to Produce Global Flood Hazard Layers'. In: *Frontiers in Earth Science* 3, p. 85. ISSN: 2296-6463. DOI: 10.3389/feart.2015.00085. URL: http://journal.frontiersin.org/Article/10.3389/feart.2015.00085/abstract.

Sanders, B. F. (2007). 'Evaluation of on-line DEMs for flood inundation modeling'. In: *Advances in Water Resources* 30.8, pp. 1831–1843. ISSN: 03091708. DOI: 10.1016/j.advwatres.2007.02.005. URL: http://linkinghub.elsevier.com/retrieve/pii/S0309170807000279.

Santillan, J. R. and M. Makinano-Santillan (2016). 'Vertical Accuracy Assessment of 30-M Resolution Alos, Aster, and Srtm Global Dems Over Northeastern Mindanao, Philippines'. In: *International Archives of the Photogrammetry, Remote Sensing and Spatial Information Sciences* XLI-B4.July. ISSN: 2194-9034. DOI: 10.5194/isprsarchives-XLI-B4-149-2016.

Schumann, G. J.-P., P. D. Bates, J. C. Neal, and K. M. Andreadis (2014). 'Fight floods on a global scale'. In: *Nature* 507.7491, pp. 169–169. DOI: 10.1038/507169e. URL: http://www.nature.com/doifinder/10.1038/507169e.

Schumann, G. J.-P., G. Di Baldassarre, D. E. Alsdorf, and P. D. Bates (2010). 'Near real-time flood wave approximation on large rivers from space: Application to the River Po, Italy'. In: *Water Resources Research* 46.5. ISSN: 00431397. DOI: 10.1029/2008WR007672.

Simpson, A. L., S. Balog, D. K. Moller, B. H. Strauss, and K. Saito (2015). 'An urgent case for higher resolution digital elevation models in the world's poorest and most vulnerable countries'. In: *Frontiers in Earth Science* 3, p. 50. ISSN: 2296-6463. DOI: 10.3389/feart.2015.00050. URL: http://journal.frontiersin.org/Article/10.3389/feart.2015.00050/abstract.

Stanski, H. R., L. J. Wilson, and W. R. Burrows (1989). *Survey of common verification methods in meteorology.* World Meteorological Organization Geneva.

Tachikawa, T., M. Hato, M. Kaku, and A. Iwasaki (2011). 'Characteristics of ASTER GDEM version 2'. In: *2011 IEEE International Geoscience and Remote Sensing Symposium*. IEEE, pp. 3657–3660. ISBN: 978-1-4577-1003-2. DOI: 10.1109/IGARSS.2011.6050017. URL: http://ieeexplore.ieee.org/document/6050017/.

Tadono, T., H. Nagai, H. Ishida, F. Oda, S. Naito, K. Minakawa, and H. Iwamoto (2016). 'Generatiojn of the 30 m-mesh global digital surface model by ALOS PRISM'. In: *ISPRS - International Archives of the Photogrammetry, Remote Sensing and Spatial Information Sciences* XLI-B4, pp. 157–162. ISSN: 2194-9034. DOI: 10.5194/isprs-archives-XLI-B4-157-2016. URL: http://www.int-arch-photogramm-remote-sens-spatial-inf-sci.net/XLI-B4/157/2016/.

Tarekegn, T. H., A. T. Haile, T. Rientjes, P. Reggiani, and D. Alkema (2010). 'Assessment of an ASTER-generated DEM for 2D hydrodynamic flood modeling'. In: *International Journal of Applied Earth Observation and Geoinformation* 12.6, pp. 457–465. ISSN: 03032434. DOI: 10.1016/j.jag.2010.05.007. URL: http://linkinghub.elsevier.com/retrieve/pii/S0303243410000620.

Trigg, M. A., C. E. Birch, J. C. Neal, P. D. Bates, A. M. Smith, C. C. Sampson, D. Yamazaki, Y. Hirabayashi, F. Pappenberger, E. Dutra, P. J. Ward, H. C. Winsemius, P. Salamon, F. Dottori, R. Rudari, M. S. Kappes, A. L. Simpson, G. Hadzilacos, and T. J. Fewtrell (2016). 'The credibility challenge for global fluvial flood risk analysis'. In: *Environmental Research Letters* 11.9, p. 094014. ISSN: 1748-9326. DOI: 10.1088/1748-9326/11/9/094014. URL: http://stacks.iop.org/1748-9326/11/i=9/a=094014?key=crossref.b898d75acc25c871d21b6be9b2ebcd65.

Wang, W., X. Yang, and T. Yao (2012). 'Evaluation of ASTER GDEM and SRTM and their suitability in hydraulic modelling of a glacial lake outburst flood in southeast Tibet'. In: *Hydrological Processes* 26.2, pp. 213–225. ISSN: 08856087. DOI: 10.1002/hyp.8127. URL: http://doi.wiley.com/10.1002/hyp.8127.

Yamazaki, D., D. Ikeshima, R. Tawatari, T. Yamaguchi, F. E. O'Loughlin, J. C. Neal, C. C. Sampson, S. Kanae, and P. D. Bates (2017). 'A high-accuracy map of global terrain elevations'. In: *Geophysical Research Letters* 44.11, pp. 5844–5853. ISSN: 00948276. DOI: 10.1002/2017GL072874. URL: http://doi.wiley.com/10.1002/2017GL072874.

Yan, K., G. Di Baldassarre, D. P. Solomatine, and G. J.-P. Schumann (2015a). 'A review of low-cost space-borne data for flood modelling: topography, flood extent and water level'. In: *Hydrological Processes* 29.15, pp. 3368–3387. ISSN: 08856087. DOI: 10.1002/hyp.10449. URL: http://doi.wiley.com/10.1002/hyp.10449.

Yan, K., A. Tarpanelli, G. Balint, T. Moramarco, and G. D. Baldassarre (2015b). 'Exploring the Potential of SRTM Topography and Radar Altimetry to Support Flood Propagation Modeling:

Danube Case Study'. In: *Journal of Hydrologic Engineering* 20.2, p. 04014048. ISSN: 1084-0699. DOI: 10.1061/(ASCE)HE.1943-5584.0001018.